INTERNATIONAL JOURNAL FOR NUMERICAL METHODS IN FLUIDS
Int. J. Numer. Meth. Fluids 2004; **44**:525–543 (DOI: 10.1002/fld.655)

Space–time integrated least squares: a time-marching approach

Olivier Besson*,† and Gautier de Montmollin

Institute of Mathematics, University of Neuchâtel, 11, rue Emile Argand, Neuchâtel 2007, Switzerland

SUMMARY

A time-marching formulation is derived from the space–time integrated least squares (STILS) method for solving a pure hyperbolic convection equation and is numerically compared to various known methods.

KEY WORDS: conservation law; space–time least square; time marching; streamline; upwind; Petrov–Galerkin; characteristics

1. INTRODUCTION

The numerical solution of the time-dependent convective transport equation by finite element methods shows recurrent problems of stability, accuracy, over- and undershootings and numerical diffusion. Independently of the question of choosing better shape functions or meshes, various attempts have been made towards space–time integration and least squares.

The least-squares method is widely used to solve partial differential equations, see References [1, 2] for elasticity and fluid mechanics problems. Few general mathematical results have been obtained for this method in the case of first-order time-dependent conservation laws. A first attempt was given in References [3–6]. In Reference [7], a mathematical analysis of this method is given for the linear conservation law and compared with renormalized solutions [8].

It seems that the space–time integrated least squares (STILS) method originated to References [9, 10]. In References [9, 11], a least square method is used to solve a 2D stationary first-order conservation equation with regularity assumptions on the advection velocity. In References [12–14], least square in space and numerical discretization in time are used to solve conservation equations.

In Section 2, a time-marching version of the STILS method is presented. In Section 3, we recall some well-known methods. In Section 4, numerical comparisons between all the presented methods are given and, in Section 5, we give some conclusions and remarks.

*Correspondence to: O. Besson, Institut de Mathematiques, Faculté des Sciences, Université de Neuchâtel, 11 rue Emile Argand, Neuchâtel CH-2007, Switzerland.
†E-mail: olivier.besson@unine.ch

Received 18 April 2002
Revised 2 June 2003

The numerical comparison is performed between the following methods:

- Space–time integrated least-squares method with time marching (STILS-TM).
- Usual finite element methods in space, with the same continuous basis functions: Galerkin, streamline diffusion, shock capturing.
- Characteristics method using a particle convection flow.

By their nature, the examples will highlight virtues and defects of all methods. Of course they will also show intrinsic difficulties of the problems. In one example the exact solution is explicitly available, providing an absolute reference. In all presented situations, the STILS-TM method gives very accurate results, with low diffusion effects and without any parameter tuning.

The problem of the numerical solution for conservation laws has been considered since a long time and many solutions have been proposed, see e.g. References [15–18] and the references therein. To our knowledge the STILS-TM method is new. Moreover, its simplicity and precision let it to be more suitable.

1.1. General equation

Let $\Omega \subset \mathbb{R}^d$ be a bounded domain with a piecewise $\mathscr{C}^1$ boundary, $v : \Omega \to \mathbb{R}^d$ a given steady-state transport velocity and $f : \Omega \times]0, T[\to \mathbb{R}^d$ a given source term.

The problem consists in finding a function $c : \Omega \times \mathbb{R}_+ \to [0, 1]$ satisfying the following partial differential equation:

$$\frac{\partial c}{\partial t} + \operatorname{div}(cv) = f \tag{1}$$

and the initial and inflow boundary conditions

$$c(x, 0) = c_0(x) \quad \text{for } x \text{ in } \Omega \tag{2}$$

$$c(x, t) = c_b(x, t) \quad \text{for } x \text{ on } \Gamma_- = \{x \in \partial\Omega : (v(x) \mid n(x)) < 0\} \tag{3}$$

where $n(x)$ is the outer normal to $\partial\Omega$ at point x.

We assume that $c_b = 0$, the general case being obtained by superposition. The function c represents for example a chemical concentration transported by an incompressible liquid flow in the domain Ω [19, 20].

The velocity v may be solution of Navier–Stokes equations. It may also derive from a potential like in our third example in Section 4.3.

2. PRESENTATION OF THE STILS METHOD

2.1. The mathematical formulation [*3, 6, 9, 10*]

Let us recall the principles of the STILS method for the transport equation (1).

In a space–time description, time is just seen as the $(d+1)$th space dimension. So, the space–time domain $\tilde{\Omega}$ can be defined as $\Omega \times]0, T[$, $T > 0$. The space–time velocity is $\tilde{v} = (v_1, \ldots, v_d, 1)$

and the space–time inflow boundary is

$$\tilde{\Gamma}_- = \{(x,t) \in \partial\tilde{\Omega} : (\tilde{v} \mid \tilde{n}) < 0\}$$

Thus, we have

$$\tilde{\Gamma}_- = (\Gamma_- \times [0,T]) \cup (\Omega \times \{0\})$$

The initial value condition inside the domain Ω (that is on $\Omega \times \{0\}$) is a part of space–time inflow boundary condition.

Starting from a divergence-free situation ($\operatorname{div} v = 0$) the transport equation (1) becomes

$$(\tilde{\nabla} c \mid \tilde{v}) = f \tag{4}$$

where $\tilde{\nabla} = (\partial/\partial x_1, \ldots, \partial/\partial x_d, \partial/\partial t)$ is the space–time gradient.

Let us define the function space

$$H(v, \tilde{\Omega}, \tilde{\Gamma}) = \{u \in L^2(\tilde{\Omega}) : (\tilde{\nabla} u \mid \tilde{v}) \in L^2(\tilde{\Omega})\}$$

equipped with the graph norm $\|u\|^2 = \|u\|_0^2 + \|(\tilde{\nabla} u \mid \tilde{v})\|_0^2$ and its underlying dot product $((u,w)) = (u,w)_0 + ((\tilde{\nabla} u \mid \tilde{v}), (\tilde{\nabla} w \mid \tilde{v}))_0$. We define the subspace

$$H_0(v, \tilde{\Omega}, \tilde{\Gamma}) = \{u \in H(v, \tilde{\Omega}, \tilde{\Gamma}) : u = 0 \text{ on } \tilde{\Gamma}_-\}$$

corresponding to a zero Dirichlet condition on the inflow boundary. The following theorem is proved in Reference [7].

Theorem 1 (*Curved Poincaré inequality* [*3, 7*])
If $v \in L^2(\Omega)^{\mathrm{d}}$ and $\operatorname{div} v = 0$, the semi-norm on $H_0(v, \tilde{\Omega}, \tilde{\Gamma})$ defined by

$$|\varphi|_{1,v} = \left(\int_{\tilde{\Omega}} (\tilde{v} \mid \tilde{\nabla} \varphi)^2 \, \mathrm{d}x \, \mathrm{d}t \right)^{1/2}$$

is a norm, equivalent to the norm on $H(v, \tilde{\Omega}, \tilde{\Gamma})$.

Let us define the linear form $\mathscr{A}u = (\tilde{\nabla} u \mid \tilde{v})$. Then Equation (4) can be written as $\mathscr{A}u = f$. In L^2, a solution of this equation corresponds to a zero of the following convex, positive functional

$$J(u) = \frac{1}{2} \int_{\tilde{\Omega}} (\mathscr{A}u - f)^2 \, \mathrm{d}x \, \mathrm{d}t$$

The STILS approach is to search for a minimum of J. We will see that under a simple regularity condition on v, we have the existence and uniqueness of such a minimum.

2.1.1. The weak formulation and well-posedness. Let us write DJ the Gâteaux derivative of the functional J on $H_0(v, \tilde{\Omega}, \tilde{\Gamma})$

$$[DJ(u)]w = \lim_{h \to 0} \frac{1}{h} (J(u + hw) - J(u))$$

Then

$$[DJ(u)]w = \int_{\tilde{\Omega}} (\mathscr{A}u - f)\mathscr{A}w \, \mathrm{d}x$$

Since J is convex, a sufficient condition to minimize J is that $[DJ(u)]w = 0$ for all w in $H_0(v, \tilde{\Omega}, \tilde{\Gamma})$ [21].

Consider now the bilinear form

$$\mathscr{B}(u, w) = \int_{\tilde{\Omega}} \mathscr{A}u\mathscr{A}w \, \mathrm{d}x \, \mathrm{d}t = \int_{\tilde{\Omega}} (\tilde{\nabla}u \,|\, \tilde{v})(\tilde{\nabla}w \,|\, \tilde{v}) \, \mathrm{d}x \, \mathrm{d}t$$

and the linear form

$$\mathscr{L}(w) = \int_{\tilde{\Omega}} f\mathscr{A}w \, \mathrm{d}x \, \mathrm{d}t = \int_{\tilde{\Omega}} f(\tilde{\nabla}w \,|\, \tilde{v}) \, \mathrm{d}x \, \mathrm{d}t$$

So $DJ(u) = 0$ if and only if

$$\mathscr{B}(u, w) = \mathscr{L}(w) \quad \text{for all } w \in H_0(v, \tilde{\Omega}, \tilde{\Gamma}_-) \tag{5}$$

The forms $\mathscr{B}$ and $\mathscr{L}$ are continuous since $|\mathscr{B}(u, w)| \leqslant \|u\| \, \|w\|$ and $|\mathscr{L}(w)| \leqslant \|f\|_0 \, \|w\|$. The *weak problem* for STILS can be stated as

$$\text{Find } u \in H_0(v, \tilde{\Omega}, \tilde{\Gamma}_-) \text{ such that (5) is satisfied} \tag{6}$$

Theorem 2 (*Well-posedness* [7])
If $v \in L^2(\Omega)^{\mathrm{d}}$ and $\operatorname{div} v = 0$, then the weak problem (6) has a unique solution; moreover, this solution holds for the strong problem (4).

2.1.2. Interpreting the weak equation. We have

$$[DJ(u)]w = \int_{\tilde{\Omega}} ((\tilde{\nabla}u \,|\, \tilde{v}) - f)(\tilde{\nabla}w \,|\, \tilde{v}) \, \mathrm{d}x = \int_{\tilde{\Omega}} ((\tilde{v} \otimes \tilde{v})\tilde{\nabla}u - f\tilde{v} \,|\, \tilde{\nabla}w) \, \mathrm{d}x \, \mathrm{d}t \tag{7}$$

The condition $DJ(u) = 0$, using formulation (7), is nothing else than the weak form of a *diffusion* problem expressed in space–time, with $(\tilde{v} \otimes \tilde{v})$ as the degenerate diffusion tensor.

Indeed, by Green's formula, we formally have

$$0 = \int_{\partial\tilde{\Omega}} ((\tilde{v} \otimes \tilde{v})\tilde{\nabla}u - f\tilde{v} \,|\, \tilde{n})w \, \mathrm{d}\gamma - \int_{\tilde{\Omega}} \widetilde{\operatorname{div}}((\tilde{v} \otimes \tilde{v})\tilde{\nabla}u - f\tilde{v})w \, \mathrm{d}x$$

for all w in $H_0(v, \tilde{\Omega}, \tilde{\Gamma}_-)$. Thus,

$$\begin{aligned} &\widetilde{\operatorname{div}}((\tilde{v} \otimes \tilde{v})\tilde{\nabla}u) = \widetilde{\operatorname{div}}(f\tilde{v}) \quad \text{in } \tilde{\Omega} \\ &((\tilde{v} \otimes \tilde{v})\tilde{\nabla}u - f\tilde{v} \,|\, \tilde{n}) = 0 \qquad \text{on } \partial\tilde{\Omega}\backslash\tilde{\Gamma}_- \end{aligned} \tag{8}$$

2.2. A time-marching version of STILS [3, 6, 22]

Let $\{\psi_1 \cdots \psi_N\}$ be a basis of a finite dimensional subspace $V_h \subset H(v, \Omega, \Gamma_-)$. Define

$$\begin{aligned} a_k(t) &= \frac{1}{\tau}(t_{k+1} - t) \\ a_{k+1}(t) &= \frac{1}{\tau}(t - t_k) \end{aligned} \tag{9}$$

with $t \in [t_k, t_{k+1}] \subset [0, T]$, $\tau = t_{k+1} - t_k$. Consider the *local problem* given in the domain $\tilde{\Omega}_k = \Omega \times]t_k, t_{k+1}[$, with an initial condition on $\Omega \times \{t_k\}$. Let E_2 be the two-dimensional subspace of $\mathscr{C}[t_k, t_{k+1}]$ generated by a_k and a_{k+1}.

An approximation of problem (6) consists in finding $c_h \in H_{0,h} = (V_h \otimes E_2) \cap H_0(v, \tilde{\Omega}_k, \tilde{\Gamma}_-)$ such that

$$\mathscr{B}(c_h, w_h) = \mathscr{L}(w_h) \quad \text{for all } w_h \in H_{0,h} \tag{10}$$

or

$$\int_\Omega \int_{t_k}^{t_{k+1}} (\tilde{\nabla} c_h \mid \tilde{v})(\tilde{\nabla} w_h \mid \tilde{v}) \, \mathrm{d}t \, \mathrm{d}x = \int_\Omega \int_{t_k}^{t_{k+1}} f(\tilde{\nabla} w_h \mid \tilde{v}) \, \mathrm{d}t \, \mathrm{d}x \tag{11}$$

for all $w_h \in H_{0,h}$, where

$$c_h(x, t) = \sum_{j=1}^{N} \psi_j(x)(a_k(t) c_j^k + a_{k+1}(t) c_j^{k+1}) \tag{12}$$

and the vector c^k contains the known state at time $t = t_k$. The problem can be written as

$$\sum_{j=1}^{N} \mathscr{B}(\psi_j a_{k+1}, \psi_i a_{k+1}) c_j^{k+1} = \mathscr{L}(\psi_i a_{k+1}) - \sum_{j=1}^{N} \mathscr{B}(\psi_j a_k, \psi_i a_{k+1}) c_j^k \tag{13}$$

After a time integration we obtain the *STILS-time-marching scheme with Q1 elements in time* (*STILS-TMQ*1)

$$\begin{aligned} &\sum_{j=1}^{N} c_j^{k+1} \int_\Omega \left[\frac{\tau}{3} (\nabla \psi_j \mid v)(\nabla \psi_i \mid v) + \frac{1}{2} (\nabla \psi_j \mid v) \psi_i + \frac{1}{2} \psi_j (\nabla \psi_i \mid v) + \frac{1}{\tau} \psi_j \psi_i \right] \mathrm{d}x \\ &\quad = \sum_{j=1}^{N} c_j^k \int_\Omega \left[\frac{-\tau}{6} (\nabla \psi_j \mid v)(\nabla \psi_i \mid v) - \frac{1}{2} (\nabla \psi_j \mid v) \psi_i + \frac{1}{2} \psi_j (\nabla \psi_i \mid v) + \frac{1}{\tau} \psi_j \psi_i \right] \mathrm{d}x + l_i \end{aligned} \tag{14}$$

for all $i \in \{1 \cdots N\}$, with the source term $l_i = \mathscr{L}(\psi_i a_{k+1})$.

In the 1D case, the jth equation has the form

$$\begin{aligned} &(1 - 2\kappa^2) u_{j-1}^{n+1} + 4(1 + \kappa^2) u_j^{n+1} + (1 - 2\kappa^2) u_{j+1}^{n+1} \\ &\quad = (1 + 3\kappa + \kappa^2) u_{j-1}^n + 2(2 - \kappa^2) u_j^n + (1 - 3\kappa + \kappa^2) u_{j+1}^n \end{aligned}$$

where $\kappa = \tau v/h$ is the Courant number. It can be seen without difficulty that this scheme is stable and that the consistency error has the form

$$E = c\left(\frac{\tau^2 v^3}{6} + \frac{\tau v^2}{24}(h^2 - 3\tau^2 v^2) + \text{h.o.t.}\right)$$

3. SOME CLASSICAL METHODS

In this section, we briefly recall some well-known methods used in our comparisons.

3.1. Continuous finite elements in space [23]

Since this family of methods is well known, we will only mention here the weak equations for the convection problem (4) and their resulting matrix components.

Let us first define $H_0 = \{u \in H^1(\Omega) : u = 0 \text{ on } \Gamma_-\}$ the basic function space having zero Dirichlet condition on the inflow boundary. Thus, the weak formulation can be written as: Find $c \in L^2(0; T; H_0)$ such that

$$\int_\Omega (\nabla c \mid v) w \, \mathrm{d}x + \int_\Omega \frac{\partial c}{\partial t} w \, \mathrm{d}x = \int_\Omega f w \, \mathrm{d}x$$

for all $w \in H_0$. If $\sum_{j=1}^N c_j(t)\psi_j(x)$ is an approximation of $c(x,t)$, the above equation leads to a differential system

$$Rc + Mc' = b$$

with $R = (r_{ij})$, $r_{ij} = \int_\Omega (\nabla \psi_j \mid v)\, \psi_i \, \mathrm{d}x$ and $M = (m_{ij})$, $m_{ij} = \int_\Omega \psi_j \, \psi_i \, \mathrm{d}x$. This basic Galerkin method is notoriously unsuited without modification for a problem with dominating hyperbolic term, due to its instability mainly around discontinuities. This is why we have implemented well-known improvements such as streamline diffusion and shock capturing. Let us recall briefly these improvements.

3.1.1. Streamline diffusion [24]. Adding diffusion artificially helps to reduce oscillations. It is better to filter the diffusion across streamlines to avoid 'infecting' nearby streamlines with wrong values. The test-function w is completed with a term $\delta(\nabla w \mid v)$, where δ is an arbitrary real number.

Then the corresponding weak formulation is

$$\int_\Omega (\nabla c \mid v)[w + \delta(\nabla w \mid v)] \, \mathrm{d}x + \int_\Omega \frac{\partial c}{\partial t}[w + \delta(\nabla w \mid v)] \, \mathrm{d}x = \int_\Omega f[w + \delta(\nabla w \mid v)] \, \mathrm{d}x \qquad (15)$$

for all $w \in H_0$. Writing $\psi_i^\delta = \psi_i + \delta(\nabla \psi_i \mid v)$, the space-discretized system becomes

$$R^\delta c + M^\delta c' = b$$

with $r_{ij}^\delta = \int_\Omega (\nabla \psi_j \mid v)\, \psi_i^\delta \, \mathrm{d}x$ and $m_{ij}^\delta = \int_\Omega \psi_j \, \psi_i^\delta \, \mathrm{d}x$.

3.1.2. Shock capturing [*23, 25, 26*]. In this case, the idea is to emphasize the previous effect when there are locally strong variations of c in the streamline direction. Let us define the projection

$$v_{//} = \begin{cases} \dfrac{(v \mid \nabla c^H)}{\|\nabla c^H\|_2^2} \nabla c^H & \text{if } \nabla c^H \neq 0 \\ 0 & \text{if } \nabla c^H = 0 \end{cases}$$

of v onto ∇c^H, where $c^H = \sum_j c_j \psi_j$ is the current approximation in space. We then combine diffusion along streamlines and the new projection, with appropriate weights. Re-using previous notation, we can write the modified basis functions as

$$\psi_i^\delta = \psi_i + \delta_1(\nabla\psi_i \mid v) + \delta_2(\nabla\psi_i \mid v_{//})$$

The ways of choosing δ_1 and δ_2 are discussed in the literature. We have implemented shock capturing with constant δ_1, δ_2 in Ω (see Section 4).

Remark that in Equation (15) or its equivalent for shock capturing, a second-order backward difference formula scheme [27] is used. The total discretization is

$$\sum_{j=1}^{N} c_j^{k+1} \int_\Omega \left[\delta(\nabla\psi_j \mid v)(\nabla\psi_i \mid v) + (\nabla\psi_j \mid v)\psi_i + \frac{3\delta}{2\tau}\psi_j(\nabla\psi_i \mid v) + \frac{3\delta}{2\tau}\psi_j\psi_i \right] \mathrm{d}x$$

$$= \sum_{j=1}^{N} \frac{1}{\tau}\left(2c_j^k - \frac{1}{2}c_j^{k-1}\right) \int_\Omega \psi_j(\psi_i + \delta\nabla\psi_i \mid v)\,\mathrm{d}x + \int_\Omega f(\psi_i + \delta\nabla\psi_i \mid v)\,\mathrm{d}x \qquad (16)$$

A comparison of Equations (16) and (14) shows that the streamline diffusion and the STILS-TM methods are totally different. The coefficient δ depends only on space, while in the STILS case it is only time dependent.

3.2. A characteristics method

For the sake of completeness, let us recall this well-known method. Let $(x^0, t_0) \in \overline{\Omega \times]0, T[}$, consider the curve $(x(t), t)$ such that $x'(t) = v(x(t), t)$. In other words, the curve (the characteristic) integrates the velocity field v. Let $c(x, t)$ be a solution of $\mathrm{div}(-cv) = \partial c/\partial t$ on $\Omega \times]0, T[$. Then we have

$$\frac{\mathrm{d}c}{\mathrm{d}t}(x(t), t) = \sum_{j=1}^{d} \frac{\partial c}{\partial x_j}\frac{\mathrm{d}x_j}{\mathrm{d}t} + \frac{\partial c}{\partial t} = \sum_{j=1}^{d} \frac{\partial c}{\partial x_j} v_j + \frac{\partial c}{\partial t}$$

$$= (\nabla c \mid v) + \frac{\partial c}{\partial t} = \mathrm{div}(cv) + \frac{\partial c}{\partial t} - c\,\mathrm{div}(v)$$

$$= f(x(t), t) - c(x(t), t)\,\mathrm{div}(v(x(t), t))$$

This shows that along the characteristic, c is a solution of a simple ODE. If the flow is incompressible and $f = 0$ then c is constant along the characteristic curves.

The numerical implementation is carried out using a particle flow. Each particle holds a value of c determined by an initial or boundary condition. In our program, the characteristics are integrated by the 8th-order Dormand–Prince [27] variable-step method. At main time steps, the values of c on nodes are estimated according to the nearby particles.

4. NUMERICAL EXPERIMENTS

Let us provide some details concerning the numerical implementation, for reproducibility. As usual, the coefficients δ_1, δ_2 in streamline and shock-capturing situations are constant. They are of about the maximum diameter of the elements. We used $\delta_1 = 0.6\delta_m/\sqrt{2}$ and $\delta_2 = 0.8\delta_m/\sqrt{2}$, where δ_m is the maximum diameter of the elements. The linear systems are solved either with a direct LU-type method—DGBTRF from the LAPACK library—with band matrices, or with (bi)-conjugate gradient iterative methods, with sparse matrices. All the tests were run on a Compaq AXP 8420 under OpenVMS. All finite element methods implemented here (including STILS-TM) use exactly the same mesh and basis functions in space. In time, for STILS-TM, the basis functions have a *lower* order than other methods where a second-order BDF time discretization is used. Even in this case, the sharpness of the results is the best for our method. In Reference [22], second-order methods have been analysed, showing a very good quality of the numerical solutions for each example.

4.1. The rotating cylinder with a slot

This example is taken from Reference [28]. The domain Ω is the square $]-1,1[^2$ and discretized in 100×100 Q_1-elements. The initial condition is

$$c(x,y,0) = \begin{cases} 1 & \text{if } (|x| > 0.05 \text{ or } y > 0.7) \text{ and } R \leqslant 0.3 \\ 0 & \text{elsewhere} \end{cases}$$

where $R = \sqrt{x^2 + (y-0.5)^2}$, the velocity field has the form $v(x,y,t) = (-y,x)$ (Figure 1) and the final time is $T = 2\pi$.

Let us present the numerical results in this situation for the solution of problem (1) using the mentioned methods.

In Table I and following, the '$\leqslant$' for the number of time steps in the characteristics method case is due to the use of variable steps for the integration.

Table I. Results for the rotating cylinder.

Method	# Time steps	Min	Max	Relative variation	CPU time (band matrix)	CPU time (sparse matrix)
`Galerkin`	800	−0.234	1.213	6.86×10^{-3}	2h13	0h41
`SUPG`	800	−0.147	1.080	8.01×10^{-5}	2h14	0h43
`SUPG-DC`	800	−0.139	1.064	8.35×10^{-6}	3h20	1h29
`STILS-TMQ1`	800	−0.261	1.239	4.29×10^{-4}	2h18	0h33
`Characteristics`	$\leqslant 2000$	0.000	1.000	1.41×10^{-2}	0h58	

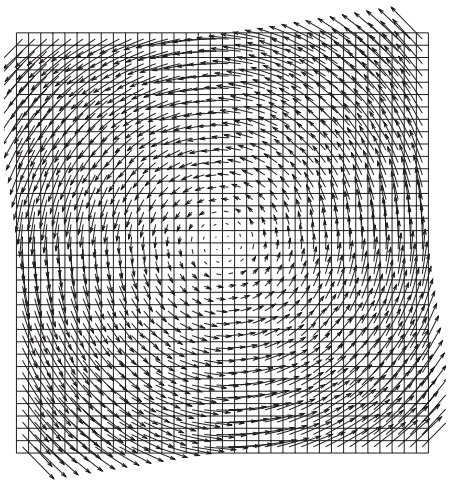

Figure 1. Velocity field (flow), coarser mesh.

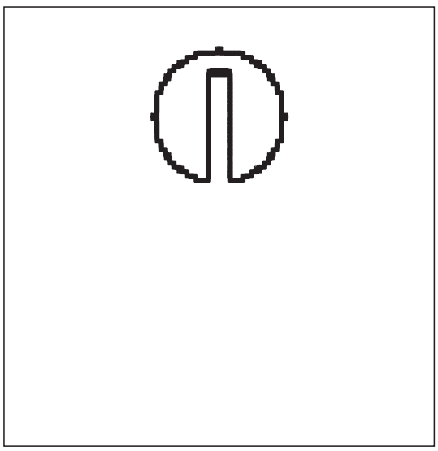

Figure 2. Initial condition, $t = 0$.

The 'relative variation' is the maximal variation of the integral concentration across the time steps, divided by the minimal value. Ideally it should be 0 since there is no source and the exact solution inside the unit disk is simply given by a rotation of the initial condition.

We present now some pictures of the numerical solutions at final time $T = 2\pi$, where the exact solution coincides with the initial condition. The figures are contour plots, and even a perfect step is displayed with a certain thickness due to interpolation made by the contouring algorithm (Figures 2–6).

We can remark that the STILS-TMQ1 scheme provides remarkable results, the shape of the slot is well preserved. The characteristics bundle is in a suitable situation and produces the

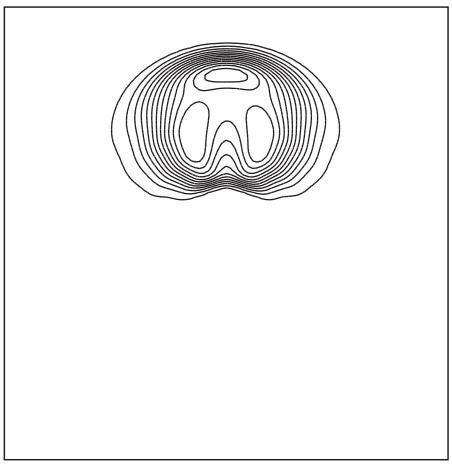

Figure 3. Streamline diffusion.

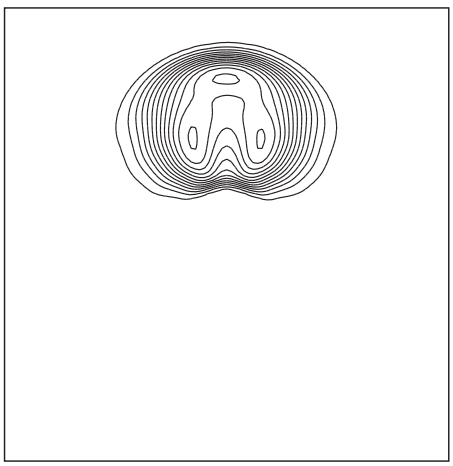

Figure 4. Streamline diffusion with shock capturing.

exact solution at each time. The streamline diffusion methods present higher diffusion effects. After all, an accurate look at Figure 5 shows some small asymmetry in the result.

4.2. The distorting flow

This problem is taken again from Reference [28] and originates from Reference [29]. It is a simulation of a distorting flow composed by several vortices with opposite directions. The domain Ω is the rectangle $]25, 75[\times]12.5, 87.5[$, discretized in 50×75 Q_1-elements. The initial

Figure 5. STILS-TMQ1.

Table II. Results for deforming flow.

Method	# Time steps	Min	Max	Relative variation	CPU time (band matrix format)
Galerkin	800	−1.032	1.140	2.52×10^{-9}	0h24
SUPG	800	−0.193	0.967	6.80×10^{-10}	0h24
SUPG-DC	800	−0.159	0.967	6.21×10^{-10}	0h38
STILS-TMQ1	800	−0.256	1.023	7.40×10^{-10}	0h25
Characteristics	$\leqslant 2000$	0.000	1.000	2.66×10^{-1}	0h26

condition is the cone

$$c(x, y, 0) = \begin{cases} 1 - R/15 & \text{if } R \leqslant 15 \\ 0 & \text{elsewhere} \end{cases}$$

where $R = \sqrt{(x-50)^2 + (y-50)^2}$. The velocity field is (Figure 7)

$$v(x, y, t) = \frac{8\pi}{25}\left(\sin\left(\frac{\pi x}{25}\right)\sin\left(\frac{\pi y}{25}\right), \cos\left(\frac{\pi x}{25}\right)\cos\left(\frac{\pi y}{25}\right)\right)$$

and final time is $T = 200 \times 1.3188 = 263.76$. All these data are taken from Reference [28]. We used 800 time steps (Table II).

As before, the theoretical relative variation is 0; moreover, the integral of the concentration over Ω is $\int_\Omega c \, \mathrm{d}x = \pi 75 \simeq 235.6$.

For each scheme, we now give the figures corresponding to the numerical solution at time $T/4$ and T (Figures 8–14).

In this example, all methods present the same kind of difficulties after a certain amount of time. The bands issued from the initial cone become more and more thin as they are coiled by the vortices, so their width end up with a thickness below the element size. The effect is a

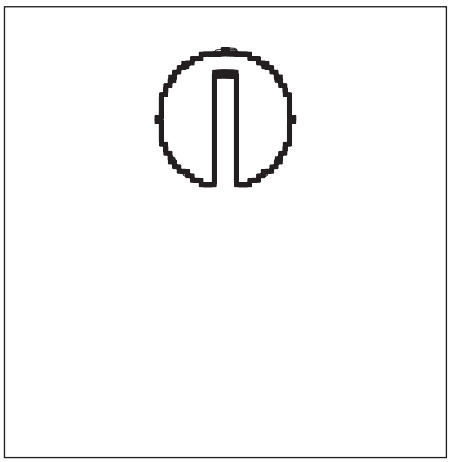

Figure 6. Characteristics.

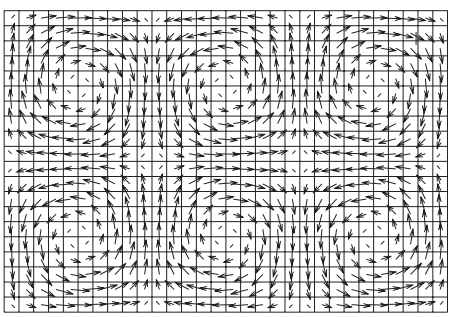

Figure 7. Velocity field (flow), coarser mesh.

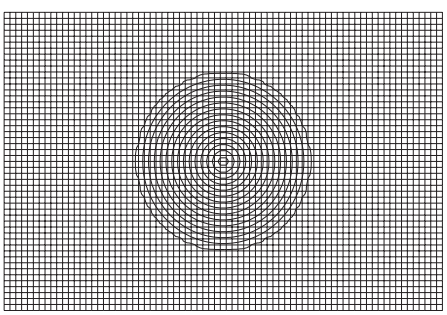

Figure 8. Initial condition.

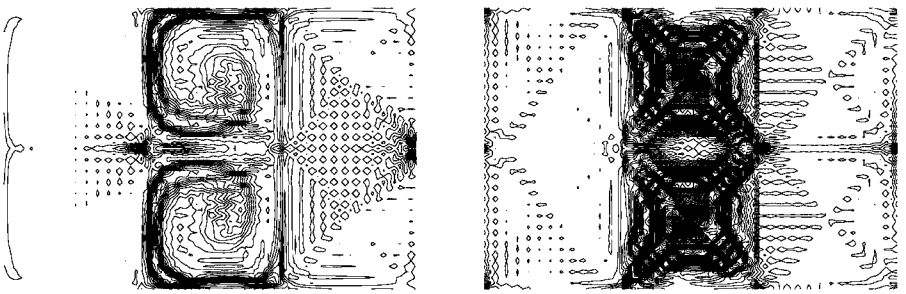

Figure 9. (a) Galerkin method (200th step). (b) Galerkin method (800th step).

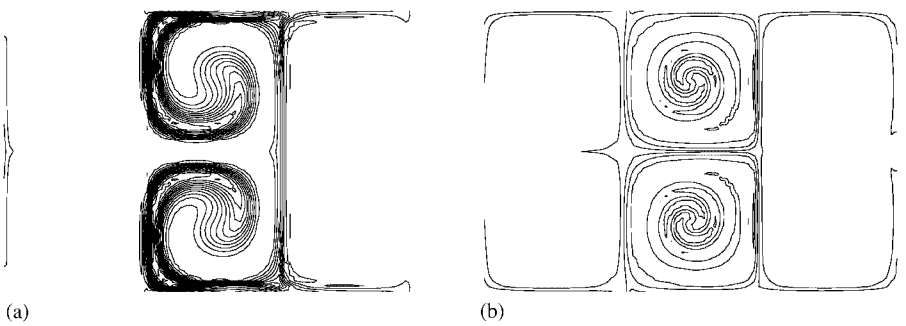

Figure 10. (a) Streamline diffusion (200th step). (b) Streamline diffusion (800th step).

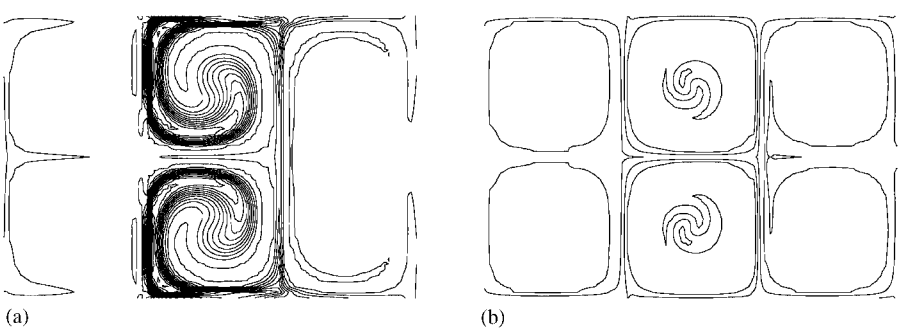

Figure 11. (a) Streamline diffusion and shock capturing (200th step). (b) Streamline diffusion and shock capturing (800th step).

complete mixing of c. However, the integral of the concentration is well preserved in any case. Again in this extreme stage, the STILS-TMQ1 method gives the best results. In Figures 10(b) and 11(b) we observe a complete diffusion of the cone, while in Figure 12(b) we can still see the coiling of the cone in the vortices, see also Figures 13(a), 13(b) and 14(a), 14(b).

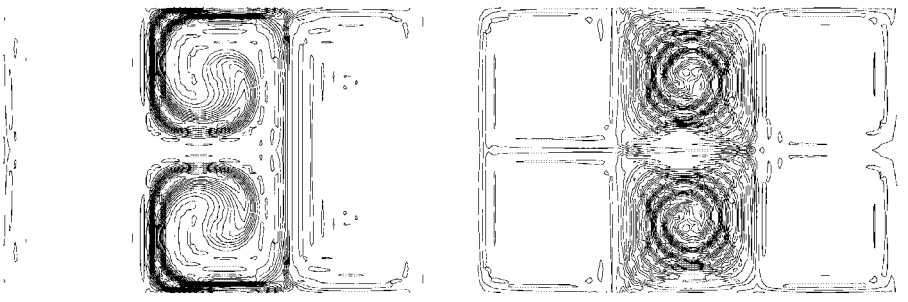

Figure 12. (a) STILS-TMQ1 (200th step). (b) STILS-TMQ1 (800th step).

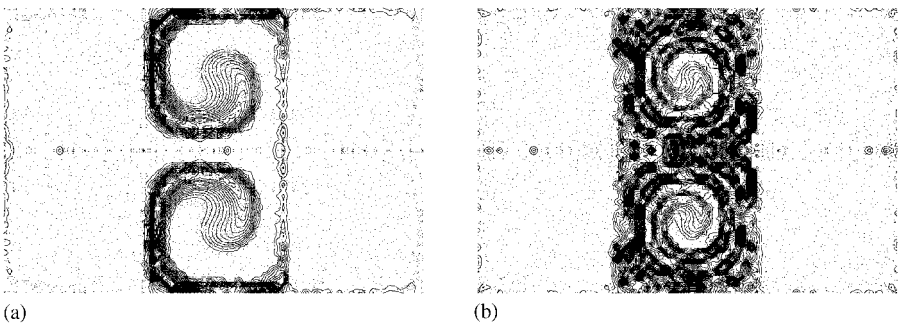

Figure 13. (a) Characteristics (200th step). (b) Characteristics (800th step).

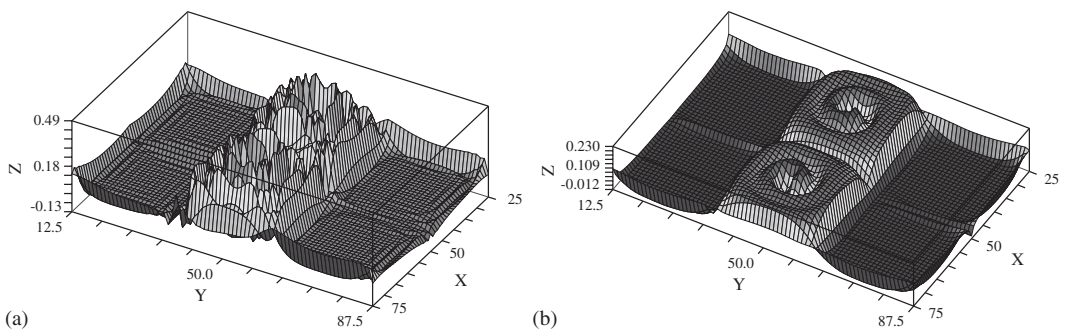

Figure 14. (a) STILS-TMQ1 (800th step). (b) Streamline diffusion and shock capturing (800th step).

4.3. The plug-flow (*see Reference* [*6*])

This example (from the above reference) is a flow and transport simulation in a groundwater medium. The domain Ω is a $20\,\mathrm{m} \times 20\,\mathrm{m}$ square and is discretized in 20×20 Q2 elements in 2D, Figure 15 illustrates the situation: a rock layer is between two conductive zones—one on the top and one on the bottom. A thin fracture cuts it in its middle and connects both zones.

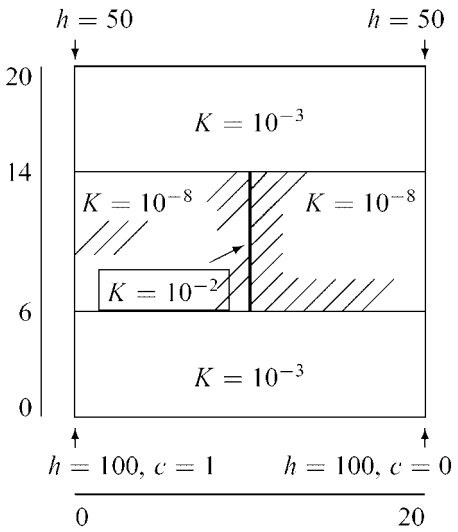

Figure 15. Permeability tensor and boundary conditions.

The velocity field v derives from a potential h that is the solution of the steady state following elliptic equation (Darcy law)

$$\operatorname{div}(K\nabla h) = 0 \tag{17}$$

where $h : \Omega \to \mathbb{R}$ is the (unknown) hydraulic head, K is the fluid conductivity tensor and $v = -K\nabla h$ is velocity vector.

The piecewise constant tensor K is defined in the following way (see Figure 15): $K = 10^{-3}$ in both conductive zones, $K = 10^{-8}$ in the rock part and $K = 10^{-2}$ in the fracture. Boundary condition is a homogeneous Neumann condition (no-flow) everywhere on $\partial\Omega$, except a Dirichlet conditions in the lower corners where $h_0 = 100$ and upper corners where $h_0 = 50$. The final time is chosen as $T = 7200$ s. This situation induces a bottom-to-top flow through the fracture. For the conservation law, the initial condition is $c = 0$ everywhere, except in the lower left corner where $c = 1$.

An important difference from the model in Reference [6] is that there is no mixture of 2D and 1D elements, nor pointwise boundary conditions. The fracture is a thin 0.2 m width rectangle and the injection points are small edges in the boundary. This is to preserve the integrity of our discretization.

Now we give the numerical results for this example (Table III).

Figure 15 describes the parameters in the problem. Figure 16 shows the level lines for the hydraulic head h.

Figures 17–19 show the level lines of the concentration c for the different methods.

Let us remark that the STILS solution, although quite stable and accurate, shows some overshootings and undershootings near the critical regions of the domain (beginning and end of the fracture). As mentioned before, the velocity field v is obtained from a finite element solution of Equation (17). In order to have a convenient approximation of the velocity v, the characteristics method was used to obtain a good refinement of the mesh near the fractures.

Table III. Results for plug flow.

Method	# Time steps	Min	Max	Final concentration	CPU time (band matrix format)
SUPG-DC	400	−3.870	4.599	114.3	1h21
STILS-TMQ1	400	−1.097	1.326	114.6	0h40
Characteristics	$\leqslant 100\,000$	0.000	1.000	104.6	5h27

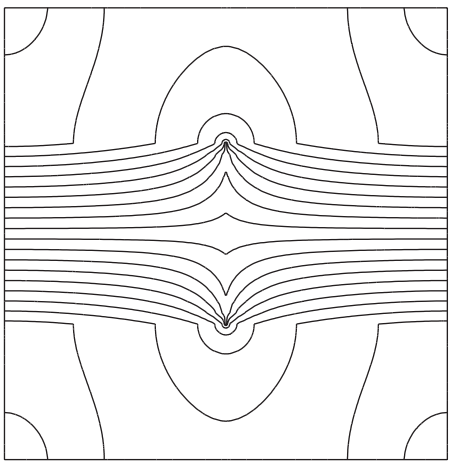

Figure 16. Level lines for h, solution of (17), from $h = 100$ to 50.

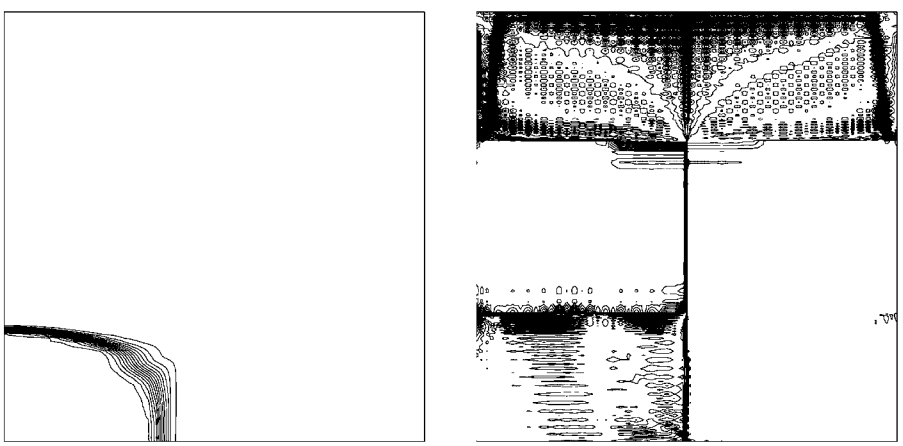

(a) (b)

Figure 17. (a) Streamline diffusion with shock capturing (100th step). (b) Streamline diffusion with shock capturing (400th step).

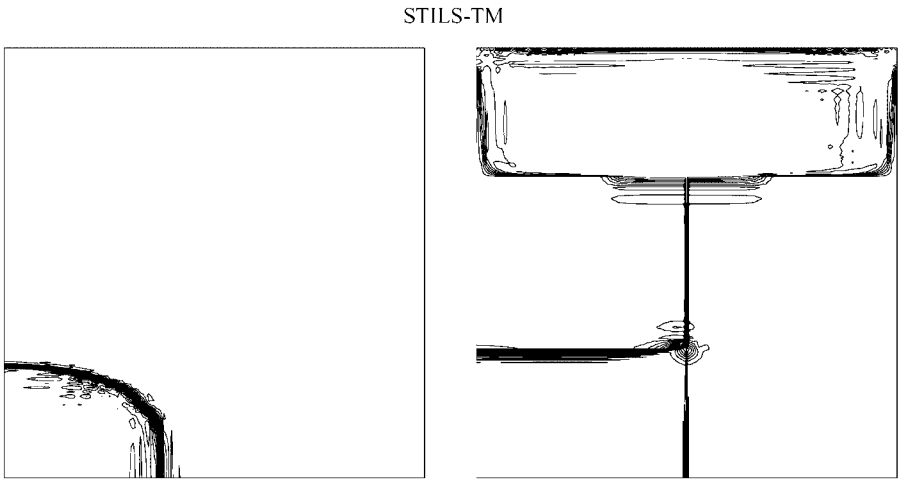

Figure 18. (a) STILS-TMQ1 (100th step). (b) STILS-TMQ1 (400th step).

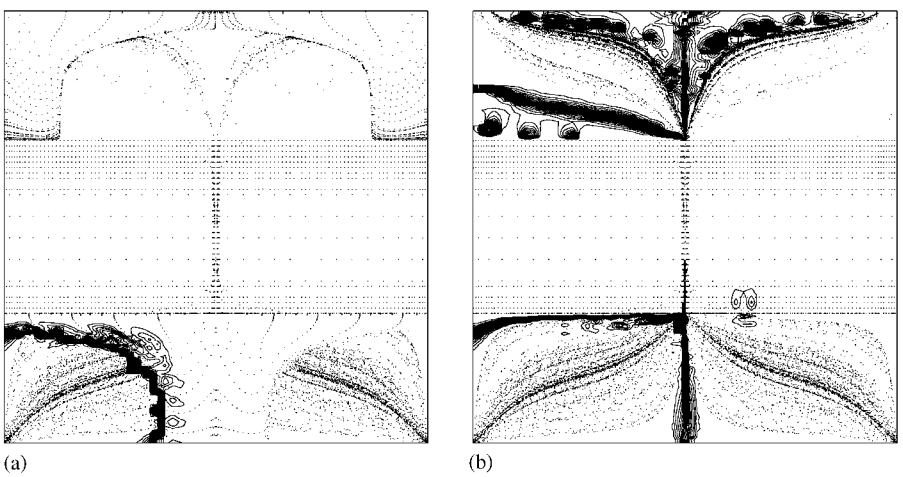

Figure 19. (a) Characteristics (100th step). (b) Characteristics (400th step).

5. CONCLUSION

In view of the previous simulations, we can do the following remarks:

1. Our scheme has obviously a better accuracy in the sense that the numerical diffusion is much smaller than for the classical finite element solutions.
2. The stability estimates presented in Reference [6] using Fourier analysis and amplification matrices show that this scheme is very stable. In the plug-flow example we can see some

overshooting near the discontinuities of the solution. This problem is common to any numerical solution of conservation laws without using slope limiter methods.

This time-marching STILS formulation, even in its simplest form in time, is very encouraging. The shape of the numerical solutions is sharper than all other analysed methods.

Still more important is that the STILS approach is beyond Galerkin methods refitted with additional terms and tuned by arbitrary parameters: it just depends on the space–time mesh and shape functions, which of course must be well chosen. This form a sane basis for further investigations. For instance, in Reference [22], quadratic finite elements in time (STILS-TMQ2) have been used and compared with the above classical methods. This method gives much better results in any case.

REFERENCES

1. Franca LP, Stenberg R. Error analysis of Galerkin least squares methods for the elasticity equations. *SIAM Journal on Numerical Analysis* 1991; **28**:1680–1697.
2. Glowinski R, Pironneau O. *Numerical Methods for Nonlinear Variational Problems.* Springer: New York, 1984.
3. Azérad P. Analyse des équations de Navier–Stokes en bassin peu profond et de l'équation de transport. *Thèse*, Université de Neuchâtel, 1996.
4. Azérad P, Pousin J. Inégalité de Poincaré courbe pour le traitement variationnel de l'équation de transport. *Comptes Rendus de l' Academic des Sciences*, *Paris*, *Series I* 1996; **322**(8):721–727.
5. Azérad P, Perrochet P, Pousin J. Space–time integrated least-squares: a simple, stable and precise finite element scheme to solve advection equations as if they were elliptic. In Progress in Partial Differential Equations: The Metz Surveys 4. Chipot M *et al.* (eds), *Proceedings of the Conference Given at the University of Metz*, *France during the 1994–95* '*Metz Days*', Pitman Research Notes on Mathematical Series, vol. 345. Longman: Harlow, 1996; 161–174.
6. Perrochet P, Azérad P. Space–time integrated least-squares: solving a pure advection equation with a pure diffusion operator. *Journal of Computational Physics* 1995; **117**:183–193.
7. Besson O, Pousin J. Hele–Shaw approximation for resin transfer molding. *Zeitschrift fur Angewandte Mathematik und Physik*, to appear.
8. Diperna RT, Lions PL. Ordinary differential equations, transport theory and Sobolev spaces. *Inventiones Mathematicae* 1989; **98**:511–547.
9. Chattot JJ, Guiu-Roux J, Lamine J. Numerical solution of first-order conservation equation by a least square method. *International Journal for Numerical Methods in Fluids* 1982; **2**:209–219.
10. Nguyen H, Reynen J. A space–time least squares finite element scheme for advection–diffusion equations. *Computer Methods in Applied Mechanics and Engineering* 1984; **42**:331–342.
11. Wilders P. On the accuracy of least square finite elements for a first-order conservation equation. *International Journal for Numerical Methods in Fluids* 1988; **8**:957–964.
12. Carey GF, Jiang BN. Least square finite elements for first-order hyperbolic systems. *International Journal for Numerical Methods in Engineering* 1988; **26**:81–93.
13. Jiang BN, Carey GF. A stable least square finite element method for non-linear hyperbolic problems. *International Journal for Numerical Methods in Fluids* 1988; **8**:933–942.
14. Chen T-F. Semidiscrete least square methods for linear hyperbolic systems. *Numerical Methods for Partial Differential Equations* 1992; **8**:423–442.
15. Godlewski E, Raviart PA. *Numerical Approximation of Hyperbolic Systems of Conservation Laws*. Springer: New York, 1996.
16. Kröner D. *Numerical Schemes for Conservation Laws*. Wiley: New York, Teubner: Stuttgart, 1997.
17. LeVeque RJ. *Numerical Methods for Conservation Laws*. Birkhäuser: Basel, 1992.
18. Morton KW. *Numerical Solution of Convection-Diffusion Problems*. Chapman & Hall: London, 1996.
19. de Marsily G. *Hydrogéologie Quantitative*. Masson: Paris, 1981.
20. Huyakorn PS, Pinder GF. *Computational Methods in Subsurface Flow*. Academic Press: New York, 1983.
21. Ciarlet P. *The Finite Element Method for Elliptic Problems*. North-Holland: Amsterdam, 1978.
22. de Montmollin G. Méthode STILS pour l'équation de transport: comparaisons et analyses. Etude d'un modèle de fermeture pour la loi de Darcy. *Thèse*, Université de Neuchâtel, 2001.
23. Johnson C. *Numerical Solution of Partial Differential Equations by the Finite Element Method*. Cambridge University Press: Cambridge, MA, 1987.
24. Hughes T. *The Finite Element Method.* Prentice-Hall: Englewood Cliffs, NJ, 1987.

25. Hughes TJR, Mallet M, Mizukami A. A new finite element formulation for computational fluid dynamics: II. Beyond SUPG. *Computer Methods in Applied Mechanics and Engineering* 1986; **54**:341–355.
26. Johnson C, Szepessy A, Hansbo P. On the convergence of shock-capturing streamline diffusion finite element methods for hyperbolic conservation laws. *European Congress on Computational Methods in Applied Sciences and Engineering*, vol. 54. 1990; 107–129.
27. Hairer E, Nørsett S, Wanner G. *Solving Ordinary Differential Equations I.* Springer: New York, 1987.
28. Hansbo P. The characteristic streamline diffusion method for convection-diffusion problems. *Computer Methods in Applied Mechanics and Engineering* 1992; **96**:239–253.
29. Smolarkiewicz PK. The multi-dimensional Crowley advection scheme. *Monthly Weather Review* 1982; **110**:1968–1983.

